Evaluation of interfacial shear stress between multi-walled carbon nanotubes and epoxy based on strain distribution measurement using Raman spectroscopy

Yashiro, Shigeki
Department of Mechanical Engineering, Shizuoka University

Sakaida, Yoshihisa
Department of Mechanical Engineering, Shizuoka University

Shimamura, Yoshinobu
Department of Mechanical Engineering, Shizuoka University

Inoue, Yoku
Department of Electronics and Materials Science, Shizuoka University

出版情報：Composites Part A: Applied Science and Manufacturing. 85, pp.192-198, 2016-03-21. Elsevier
バージョン：
権利関係：

Composites: Part A 85 (2016) 192–198
DOI: 10.1016/j.compositesa.2016.03.019

Evaluation of interfacial shear stress between multi-walled carbon nanotubes and epoxy based on strain distribution measurement using Raman spectroscopy

Shigeki Yashiro [a,*], Yoshihisa Sakaida [a], Yoshinobu Shimamura [a], Yoku Inoue [b]

[a] Department of Mechanical Engineering, Shizuoka University

[b] Department of Electronics and Materials Science, Shizuoka University

*Corresponding author: Tel: +81-53-478-1026; Fax: +81-53-478-1026.

E-mail address: yashiro.shigeki@shizuoka.ac.jp (S. Yashiro)

Abstract

This study investigated the stress recovery of aligned multi-walled carbon nanotubes (MWCNTs) embedded in epoxy using Raman spectroscopy, and evaluated interfacial shear stress between MWCNTs and epoxy using shear-lag analysis. To this end, ultralong aligned MWCNTs (3.8 mm long) were embedded in epoxy to obtain Raman spectra at multiple points along the MWCNTs. Downshift of the G'-band due to tensile strain was measured from the nanotube end to the center, and the strain distribution of embedded MWCNTs was evaluated successfully. Interfacial shear stress was then estimated by minimizing the error between the shear-lag analysis and measured strain distribution. The maximum interfacial shear stress between the embedded MWCNTs and epoxy was 10.3–24.1 MPa at the failure strain of aligned MWCNT-reinforced epoxy composites (0.46% strain). Furthermore, the interfacial shear stress

between an individual MWCNT and epoxy was investigated.

Keywords: A. Carbon nanotubes and nanofibers; A. Nanocomposites; B. Stress transfer; Raman spectroscopy

1. Introduction

Although carbon nanotubes (CNTs) are generally stiffer and stronger than carbon fibers, the major objective of earlier studies on CNT-reinforced composite materials was to improve properties of resin or to functionalize it, rather than to achieve high stiffness and/or strength. Random orientation, aggregation, and low content (a few vol.%) of CNTs were obstacles to overcome [1]. In recent years, multi-walled carbon nanotubes (MWCNTs) that can be spun into a yarn were developed [2-8] and used as a preform of aligned MWCNT-reinforced polymer composites to achieve good mechanical properties [9,10].

The interfacial properties between fibers and matrix affect the strength of the entire composite. The interfacial strength between CNTs and polymer has been measured using nano-pull-out tests [11-18]. Barber et al. [14] pulled out an individual MWCNT, which was attached to the end of an atomic force microscope chip, from epoxy and determined the interfacial shear strength to be 30±7 MPa. Ganesan et al. [17] developed a micro-fabricated device for pull-out experiments of an MWCNT, and obtained the interfacial shear strength (1.8–12.5 MPa) between an individual MWCNT and epoxy. Tsuda et al. [18] pointed out that van der Waals force was a dominant factor of interfacial bonding in the MWCNT/PEEK system. MWCNT

spun yarns have been applied to single-fiber composite tests [19,20] and micro-droplet tests [21] to estimate the interfacial property between MWCNTs and epoxy. Although many nanotube ends existed in a spun yarn, the estimated interfacial shear strength (12–20 MPa [19] and 14.4 MPa [21]) was comparable to that obtained using pull-out tests of an individual MWCNT. However, the interfacial properties between MWCNTs and polymer matrix remain unclear because of the wide variety of experiment results and uncertainty about the influence of nanotube ends in the use of spun yarns.

Successive fragmentation of fibers occurs in a long-fiber composite with increasing applied stress, and clusters of fiber breaks induce final failure of the overall composite [22]. Tensile stress in a broken fiber is zero at the break point and increases with increasing distance from the fiber break by stress transfer of surrounding matrix. Characteristic of this stress recovery affects fragmentation of an individual reinforcing fiber, and eventually strength of the overall composite.

The interfacial properties between carbon fibers and epoxy have been investigated by measuring the stress distribution of fibers based on the stress-induced Raman-band shift caused by change in the inter-atomic distance [23-27]. CNTs also have Raman spectra similar to those of carbon fibers, and the characteristic peaks shift with tensile strain [28]. Previous studies of Raman spectroscopy for CNT-distributed polymer composites have attempted to estimate the Young's modulus of an individual CNT [28], and two-dimensional strain distribution mapping near a glass fiber and a carbon fiber [29]. Debonding of CNTs from polymer matrix has been

detected using in situ Raman spectroscopy, in which a plateau in the Raman-band downshift was measured while increasing applied strain [30-32]. An approach similar to that of conventional carbon fibers can be applied to estimate the interfacial properties between CNTs and polymer; however, to the authors' knowledge, no study has measured stress recovery of CNTs because of difficulty in synthesizing CNTs elongated enough to be observed using a Raman microscope.

This study aims to evaluate the stress distribution of MWCNTs using Raman spectroscopy and to investigate the interfacial shear stress between the MWCNT and epoxy. To this end, ultralong and aligned MWCNTs [5,8] are used to achieve multi-point measurement of Raman spectra in MWCNTs. This study is organized as follows. Section 2 presents experiments that measure the strain distribution of embedded MWCNTs using Raman microscopy. Section 3 evaluates the interfacial shear stress between an aligned MWCNT bundle and epoxy using shear-lag analysis. Finally, section 4 discusses the interfacial shear stress between an individual MWCNT and epoxy.

2. Experiments

2.1 Materials

Ultralong MWCNTs aligned vertically on a quartz substrate were used in this study. Figure 1 presents an SEM image of the MWCNT array. MWCNTs were 3.8 mm long and had a diameter of 50 nm. These MWCNTs were synthesized from acetylene gas using a catalyst of

iron chloride by thermal chemical vapor deposition on a bare quartz surface. The synthesizing method is described in detail elsewhere [5,8]. A tiny part of the array (i.e., an aligned MWCNT bundle) was picked up and embedded in epoxy. Unlike CNT spun yarns (e.g., Deng [19]), nanotube ends did not exist in the middle of an MWCNT bundle, and this ensured uniform stress recovery of all MWCNTs.

Figure 2 illustrates the dimensions of the specimen. An aligned MWCNT bundle was embedded in epoxy and was loaded in tension. Bisphenol-A epoxy resin (jER 828, Mitsubishi Chemical) and curing agent triethylenetetramine (jER TETA, Mitsubishi Chemical) were used along with the diluent ethanol, and the weight ratio was 100:11:1. Here, ethanol was added to facilitate void removal. The epoxy resin was first cured at 50°C for 60 minutes, and then further cured at 100°C for 80 minutes. The influence of residual ethanol was not considered in this study. Coupon specimens with an aligned MWCNT bundle were 40 mm long, 6 mm wide, and 1.45 mm thick. The cross-section of an MWCNT bundle was almost round as depicted in Fig. 2c. Some specimens were loaded in tension until final failure, and Fig. 2d presents a typical SEM image of a fractured specimen. This SEM image indicated that epoxy was infiltrated well into the MWCNT bundle. It is noted that embedding an MWCNT bundle away from the specimen surface was ideal for stress recovery. However, the MWCNT bundle was embedded near the surface to obtain sufficient intensity of the Raman scattering light.

Two epoxy specimens without MWCNTs were also loaded in tension up to 0.3% applied strain to obtain the Young's modulus and Poisson's ratio, where the longitudinal and lateral

strains were measured simultaneously. The Young's modulus of the epoxy, E_m, was 2.93 GPa, and its Poisson's ratio, v_m, was 0.378.

2.2 Raman spectroscopy

The Raman spectra of MWCNTs embedded in epoxy were obtained using a Raman microscope (XploRA, Horiba). Table 1 lists the measurement conditions. The incident light was polarized parallel to the MWCNT alignment. The Raman spectrum of MWCNTs is depicted in Fig. 3, along with that of pure epoxy. Characteristic peaks of CNTs (D-band at 1350 cm^{-1}, G-band at 1580 cm^{-1}, and G'-band at 2700 cm^{-1}) were observed. Although the D-band and the G-band overlapped with large peaks of epoxy, no large peak of epoxy was observed near the G'-band. Therefore, downshift of the G'-band was investigated in this study. The spectrum of epoxy alone was subtracted from that of the MWCNT bundle (i.e., MWCNTs with infiltrated epoxy) to obtain the Raman spectrum of pure MWCNTs (Fig. 4). This G'-band peak was fitted to a Gaussian and Lorentzian curve to identify the peak wavenumber.

First, the downshift trend of the G'-band due to tensile strain was evaluated. Specimens were loaded in tension using a tension stage (TST350, Linkam Scientific Instruments), while the applied strain was measured using a strain gage attached near the MWCNT bundle. Both of the crossheads of this machine were moved the same distance, and the observed position was constant. Raman spectra were measured at strain levels up to an applied force of 200 N (23 MPa applied stress). The measurement was repeated at least five times for one strain level.

Figure 5 plots the peak wavenumber of the G'-band against the applied strain. The peak wavenumber decreased linearly with increasing strain. The relationship between peak wavenumber κ (cm^{-1}) and dimensionless applied strain ε was approximated by

$$\kappa = -455.7\varepsilon + 2700 . \quad (1)$$

Equation (1) enabled us to evaluate the strain of MWCNTs at an arbitrary point from the measured wavenumber of the G'-band.

The peak wavenumber of the G'-band was 2697.654 cm^{-1} before embedding (Fig. 3a), and therefore, Eq. (1) suggested that the residual strain of -0.51% was generated in the MWCNT bundle. But hereafter, the residual strain was disregarded for simplicity.

2.3 Measurement of stress recovery in the aligned MWCNT bundle

The strain distribution of an aligned MWCNT bundle was investigated. Raman spectra were first measured at pre-determined positions of the bundle without loading. The specimen was then loaded, and Raman spectra were again measured at the same pre-determined positions under constant tensile strain. The measurement was repeated at least twice for one position, and the peak wavenumber was averaged. Based on Eq. (1), strain at a position was obtained from the difference in peak wavenumbers to remove error caused by the small fluctuation of the initial peak wavenumber along the MWCNT bundle.

Figure 6 depicts a typical result of the distribution of the G'-band downshift amount along the MWCNT bundle. The horizontal axis represents the distance ratio from the center of the

bundle, x/L, where x is a coordinate whose origin is the center of the bundle and L is the half-length of the bundle. The calculated strain is also presented in the second vertical axis of Fig. 6. The strain was zero at the end of the bundle, and increased to a constant strain when approaching the center of the bundle; this result demonstrated stress recovery of the MWCNT bundle. The applied strain was about 0.5% in this test as listed in Table 2, and the epoxy was almost elastic in this strain range. Although matrix-yielding occurred in a tiny region near the end of the bundle, its influence on the strain distribution would be trivial. Epoxy has viscoelastic nature, but its influence is not significant at the room temperature. We assumed that the strain distribution did not alter within a time period required for the measurement.

Eight specimens were tested in this study. The interfacial properties will be investigated further by using the results of the four specimens in which the recovered strain almost coincided with the applied strain.

3. Evaluation of interfacial shear stress between the MWCNT bundle and epoxy

Aligned MWCNTs and resin infiltrated into the bundle behave as a unified body, and all MWCNTs in a bundle are assumed to have the same strain distribution. Thus, stress recovery along the bundle can be analyzed using a shear-lag model [33]. The longitudinal strain of the bundle, ε_f, is calculated by

$$\varepsilon_f = \varepsilon_{app}\left[1-\cosh\left(\frac{nx}{r}\right)\operatorname{sech}(ns)\right], \tag{2}$$

and the constant n is expressed as

$$n = \left[\frac{E_m}{E_{UD}(1+\nu_m)\ln(R/r)} \right]^{1/2}. \quad (3)$$

Here, x is the position from the center as illustrated in Fig. 2b, ε_{app} is the applied strain, r is the radius of the bundle, s is the aspect ratio (=L/r), E_{UD} is the Young's modulus of the aligned-MWCNT composite, E_m is the Young's modulus of the matrix resin, and ν_m is Poisson's ratio of the matrix resin. The volume fraction of MWCNTs in the bundle (4%) was determined from the weight change of an MWCNT bundle/epoxy composite measured using a thermal analyzer (DTG-60A, Shimadzu Corporation), in which epoxy alone was removed from the composite at high temperature. E_{UD} was then calculated using the rule of mixture with the estimated Young's modulus of an individual MWCNT (680 GPa) [34]. The dimensionless parameter (R/r) represents the size of the shearing zone of the matrix that transfers the tensile load to the fiber, where R is the radius accompanying shear deformation. However, the shearing zone was unclear in the experiment, and the constant n cannot be determined experimentally.

The constant n was then determined to minimize the error between the measured strain distribution and the theoretical one. Figure 6 plots the theoretical strain distribution (solid line) and the experiment result. The measured strain distribution agreed well with the theory. This consistency validated the first assumption that the MWCNT bundle and epoxy impregnated into the bundle could be considered a unidirectional composite.

The interfacial shear stress between the MWCNT bundle and the surrounding epoxy, τ_i, is

expressed as

$$\tau_i = \frac{n\varepsilon_{app}}{2} E_{UD} \sinh\left(\frac{nx}{r}\right)\mathrm{sech}(ns). \quad (4)$$

Figure 7 presents the distribution of the interfacial shear stress analyzed using the constant n determined for the specimen investigated in Fig. 6. The maximum shear stress was predicted at the end of the bundle, and the shear stress decreased to zero when approaching its center.

The fracture surfaces of aligned MWCNT-reinforced epoxy composites [9,10] suggested that fiber breaks induced the final failure of composites, and that the MWCNT/epoxy interface was intact until final failure. The failure strain of the aligned MWCNT-reinforced epoxy composite with the MWCNT volume fraction of 4.5% was 0.46% strain [34], and the maximum interfacial shear stress at that strain was 24.1 MPa. Table 2 lists the analyzed results for four specimens, and the maximum interfacial shear stress was estimated to be 10.3–24.1 MPa at 0.46% applied strain. Note that this strain was not the applied strain at which debonding was generated in the MWCNT-bundle/epoxy specimen tested in this study.

The residual strain acting on the MWCNT bundle was disregarded in this analysis. Consideration of the residual strain is a future work.

4. Discussion

The above estimation was the interfacial shear stress between the MWCNT bundle and epoxy, not between an individual MWCNT and epoxy. The maximum shear stress always appears at

the end of nanotubes ($x = L$), and an individual MWCNT has a very high aspect ratio (s = 76,000 in this study). In these conditions, the maximum interfacial shear stress can be calculated as

$$\tau_{i,\max} = \frac{n\varepsilon_{app}}{2} E_{UD} \,. \tag{5}$$

If the stress state is similar regardless of bundle diameter (i.e., the dimensionless parameter (R/r) representing shearing zone size is constant), the maximum interfacial shear stress can easily be calculated.

To verify the above assumption, the stress distribution near a homogenized fiber bundle was analyzed using the finite-element method. Figure 8 depicts an axisymmetric half-model with a bundle radius of 60 μm, considering symmetry. The model was 3 mm long, and the half-length of the bundle was 1.9 mm. Some models with a smaller bundle radius (as well as model width) were also prepared. The entire model was divided uniformly by four-node axisymmetric elements. Double-nodes were arranged at the top of the bundle, and tensile stress could not be transferred from the matrix to the bundle through the top of the bundle. Material properties as in the shear-lag analysis were used, and the Poisson's ratio of the bundle was assumed to be equal to that of the matrix. The bottom of the model was fixed in the longitudinal (x) direction, and uniform tensile displacement (0.5% strain) was applied to the top of the model.

Figure 9a depicts the contour plot of the shear strain (γ_{rx}) for the bundle radius of 60 μm, and Fig. 9b presents the shear strain γ_{rx} at the top of the bundle (x = 1.9 mm) against the distance from the center. The shear strain was concentrated at the corner of the bundle, and decreased quickly to zero. Here, the shearing zone radius R was defined as the distance from the center at

which the shear strain was less than the threshold (0.05%). Figure 10 plots the dimensionless parameter (R/r) against the bundle radius. The parameter (R/r) was roughly constant, regardless of bundle radius.

This result confirmed the use of the constant n for the MWCNT bundle (Table 2) in Eq. (5) to estimate the maximum interfacial shear stress between an individual MWCNT and epoxy. The maximum shear stress between an individual MWCNT and epoxy, $\tau_{i,max}$, was thus evaluated as 10.5 to 24.2 MPa at the applied strain of 0.46%. The estimated maximum interfacial shear stress was comparable to the interfacial shear strength measured using nano-pull-out tests [14,17] and to the interfacial shear stress between MWCNT spun yarn and epoxy estimated using the Kelly-Tyson model [19].

The MWCNT bundle was embedded near the top surface of the specimen as depicted in Fig. 2c, and the its position may affect stress transfer. Insufficient shearing zone will cause incomplete stress recovery of the MWCNT bundle. However, in the experiments, the recovered strain in the bundle almost coincided with the applied strain (Fig. 6). This result suggested that the influence of the embedding position was not so significant. Although the distance between the top surface and the MWCNT bundle was small compared to the shearing zone size, the bundle was surrounded by sufficient matrix for stress recovery, except the limited region.

5. Conclusion

This study measured the strain distribution of aligned MWCNTs embedded in epoxy based

on the downshift of the Raman G'-band, and evaluated the interfacial shear stress between MWCNTs and epoxy. An ultralong MWCNT bundle (3.8 mm long) was used in this study to achieve multi-point measurement of Raman spectra of MWCNTs. The stress recovery of the embedded MWCNT bundle was measured successfully based on the experimentally determined relationship between the peak wavenumber of the G'-band and the applied strain.

The interfacial shear stress distribution was estimated by minimizing the error between the shear-lag analysis and the measured strain distribution. The maximum interfacial shear stress between an MWCNT bundle and epoxy was 10.3 to 24.1 MPa at the failure strain of aligned MWCNT-reinforced epoxy composites (0.46% strain [34]).

Moreover, finite-element analysis was performed to predict shearing zone size, and the shear strain distribution against the distance normalized by the bundle radius was almost unchanged by the bundle diameter. This result confirmed that the ratio of bundle radius to matrix shearing zone size was almost constant. Therefore, the interfacial shear stress between an individual MWCNT and epoxy could be estimated using shear-lag analysis and the measured strain distribution of the MWCNT bundle. The maximum interfacial shear stress between an individual MWCNT and epoxy was then determined to be 10.5 to 24.2 MPa.

Acknowledgement

This research is supported by Japan Science and Technology Agency through the "Advanced Low Carbon Technology Research and Development Program (ALCA)". The authors thank Mr.

Kousei Kawamura (Shizuoka University) for his efforts in the experiment.

References

[1] Xie XL, Mai YW, Zhou XP. Dispersion and alignment of carbon nanotubes in polymer matrix: A review. Mater Sci Eng R 2005; 49:89-112.

[2] Jiang K, Li Q, Fan S. Spinning continuous carbon nanotube yarns. Nature 2002; 419:801.

[3] Zhang M, Atkinson KR, Baughman RH. Multifunctional carbon nanotube yarns by downsizing an ancient technology. Science 2004; 306:1358-1361.

[4] Motta M, Li YL, Kinloch I, Windle A. Mechanical properties of continuously spun fibers of carbon nanotubes. Nano Lett 2005; 5: 1529-1533.

[5] Inoue Y, Kakihata K, Hirono Y, Horie T, Ishida A, Mimura H. One-step grown aligned bulk carbon nanotubes by chloride mediated chemical vapor deposition. Appl Phys Lett 2008; 92:213113.

[6] Zhang S, Zhu L, Minus ML, Han Gi Chae, Jagannathan S, Wong CP, Kowalik J, Roberson LB, Kumar S. Solid-state spun fibers and yarns from 1-mm long carbon nanotube forests synthesized by water-assisted chemical vapor deposition. J Mater Sci 2008; 43: 4356-4362.

[7] Tran CD, Humphries W, Smith SM, Huynh C, Lucas S. Improving the tensile strength of carbon nanotube spun yarns using a modified spinning process. Carbon 2009; 47: 2662-2670.

[8] Ghemes A, Minami Y, Muramatsu J, Okada M, Mimura H, Inoue Y. Fabrication and

mechanical properties of carbon nanotube yarns spun from ultra-long multi-walled carbon nanotube arrays. Carbon 2012; 50:4579-4587.

[9] Ogasawara T, Moon SY, Inoue Y, Shimamura Y. Mechanical properties of aligned multi-walled carbon nanotube/epoxy composites processed using a hot-melt prepreg method. Compo Sci Technol 2011; 71:1826-1833.

[10] Shimamura Y, Oshima K, Tohgo K, Fujii T, Shirasu K, Yamamoto G, Hashida T, Goto K, Ogasawara T, Naito K, Nakano T, Inoue Y. Tensile mechanical properties of carbon nanotube/epoxy composite fabricated by pultrusion of carbon nanotube spun yarn preform. Compos Part A 2014; 62:32-38.

[11] Cooper CA, Cohen SR, Barber AH, Wagner HD. Detachment of nanotubes from a polymer matrix. Appl Phys Lett 2002; 81:3873-3875.

[12] Barber AH, Cohen SR, Wagner HD. Measurement of carbon nanotube–polymer interfacial strength. Appl Phys Lett 2003; 82:4140-4142.

[13] Barber AH, Cohen SR, Kenig S, Wagner HD. Interfacial fracture energy measurements for multi-walled carbon nanotubes pulled from a polymer matrix. Compos Sci Technol 2004; 64:2283-2289.

[14] Barber AH, Cohen SR, Eitan A, Schadler LS, Wagner HD. Fracture transitions at a carbon-nanotube/polymer interface. Adv Mater 2006; 18:83-87.

[15] Ding W, Calabri L, Kohlhaas KM, Chen X, Dikin DA, Ruoff RS. Modulus, fracture strength, and brittle vs. plastic response of the outer shell of arc-grown multi-walled carbon

nanotubes. Exp Mech 2007; 47:25-36.

[16] Manoharan MP, Sharma A, Desai AV, Haque MA, Bakis CE, Wang KW. The interfacial strength of carbon nanofiber epoxy composite using single fiber pullout experiments. Nanotechnology 2009; 20:295701.

[17] Ganesan Y, Peng C, Lu Y, Loya PE, Moloney P, Barrera E, Yakobson BI, Tour JM, Ballarini R, Lou J. Interface toughness of carbon nanotube reinforced epoxy composites. ACS Appl Mater Interfaces 2011; 3:129-134.

[18] Tsuda T, Ogasawara T, Deng F, Takeda N. Direct measurements of interfacial shear strength of multi-walled carbon nanotube/PEEK composite using a nano-pullout method. Compos Sci Technol 2011; 71:1295-1300.

[19] Deng F, Lu W, Zhao H, Zhu Y, Kim B-S, Chou T-W. The properties of dry-spun carbon nanotube fibers and their interfacial shear strength in an epoxy composite. Carbon 2011; 49:1752-1757.

[20] Liu Y-N, Li M, Gu Y, Zhang X, Zhao J, Li Q, Zhang Z. The interfacial strength and fracture characteristics of ethanol and polymer modified carbon nanotube fibers in their epoxy composites. Carbon 2013; 52:550-558.

[21] Zu M, Li Q, Zhu Y, Dey M, Wang G, Lu W, Deitzel JM, Gillespie Jr. JW, Byun J-H, Chou T-W. The effective interfacial shear strength of carbon nanotube fibers in an epoxy matrix characterized by a microdroplet test. Carbon 2012; 50:1271-1279.

[22] Okabe T, Ishii K, Nishikawa M, Takeda N. Prediction of tensile strength of unidirectional

CFRP composites. Adv Compos Mater 2010; 19:229-241.

[23] Miyake T, Yamakawa T, Ohno N. Measurement of stress relaxation in broken fibers embedded in epoxy using Raman spectroscopy. J Mater Sci 1998; 33:5177-5183.

[24] Yallee RB, Young RJ. Evaluation of interface fracture energy for single-fibre composites. Compos Sci Technol 1998; 58:1907-1916.

[25] van den Heuvel PWJ, Peijs T, Young RJ. Failure phenomena in two-dimensional multi-fibre microcomposites. Part 4: a Raman spectroscopic study on the influence of the matrix yield stress on stress concentrations. Compos Part A 2000; 31:165-171.

[26] Montes-Morán MA, Martínez-Alonso A, Tascón JMD, Young RJ. Effects of plasma oxidation on the surface and interfacial properties of ultra-high modulus carbon fibres. Compos Part A 2001; 32:361-371.

[27] Montes-Morán MA, Young RJ. Raman spectroscopy study of high-modulus carbon fibres: effect of plasma-treatment on the interfacial properties of single-fibre-epoxy composites Part II: Characterisation of the fibre-matrix interface. Carbon 2002; 40:857-875.

[28] Cooper CA, Young RJ, Halsall M. Investigation into the deformation of carbon nanotubes and their composites through the use of Raman spectroscopy. Compos Part A 2001; 32:401-411.

[29] Zhao Q, Wagner HD. Two-dimensional strain mapping in model fiber-polymer composites using nanotube Raman sensing. Compos Part A 2003; 34:1219-1225.

[30] Mu M, Osswald S, Gogotsi Y, Winey KI. An in situ Raman spectroscopy study of stress

transfer between carbon nanotubes and polymer. Nanotechnology 2009; 20:335703.

[31] Roy D, Bhattacharyya S, Rachamim A, Plati A, Saboungi M-L. Measurement of interfacial shear strength in single wall carbon nanotubes reinforced composite using Raman spectroscopy. J Appl Phys 2010; 107:043501.

[32] Newcomb BA, Chae HG, Gulgunje PV, Gupta K, Liu Y, Tsentalovich DE, Pasquali M, Kumar S. Stress transfer in polyacrylonitrile/carbon nanotube composite fibers. Polymer 2014; 55:2734-2743.

[33] Hull D, Clyne TW. An Introduction to Composite Materials Second Edition, Cambridge University Press, 1996.

[34] Ogasawara T, Nakamoto K, Tsuda T, Ogawa T, Moon SY, Shimamura Y, Inoue Y. Mechanical properties of aligned carbon nanotube/epoxy composites, Journal of the Japan Society for Composite Materials 39: 240-247, 2013. (in Japanese).

Figure captions and Table captions

Figure 1 SEM image of the ultralong MWCNT array on a quartz substrate.

Figure 2 Specimen with an embedded MWCNT bundle: (a) dimensions, (b) magnified illustration near the MWCNT bundle, (c) micrograph of the cross-section, and (d) SEM observation of a fractured MWCNT bundle embedded in epoxy.

Figure 3 Typical Raman spectra in the range of 1000 to 3000 cm^{-1}: (a) MWCNTs. (b) Epoxy.

Figure 4 Raman spectra near the G'-band of (a) pure MWCNTs, (b) the aligned-MWCNT bundle/epoxy composite, and (c) epoxy only.

Figure 5 Relationship between the Raman shift of the G'-band and the applied strain.

Figure 6 Measured and analyzed stress recovery of the aligned MWCNT bundle under 0.489% applied strain.

Figure 7 Predicted interfacial shear stress distribution corresponding to Fig. 4 (ε_{app} = 0.489%).

Figure 8 Axisymmetric finite-element model with a bundle radius of 60 μm. Some models with smaller bundle radiuses were also analyzed.

Figure 9 Shear strain (γ_{rx}) distribution near the bundle.

Figure 10 Relationship between the dimensionless parameter (R/r) and bundle radius.

Table 1 Measurement conditions for micro Raman spectroscopy.

Laser power (mW)	16.2
Laser wavelength (nm)	532
Spot size (μm)	2.6
Laser power reduction (%)	10
Exposure time (s)	70
Integration count	2
Grating (gratings/mm)	2400

Table 2 Analyzed results of the maximum interfacial shear stress between the MWCNT bundle and epoxy.

Bundle radius r (μm)	Aspect ratio s	Constant n	Applied strain in the experiment (%)	Maximum interfacial shear stress (MPa) (*)
135	14.4	0.264	0.481	18.2
116	14.7	0.209	0.452	14.4
117	16.2	0.350	0.489	24.1
119	16.0	0.152	0.444	10.3

(*) The maximum interfacial stress was calculated using the applied strain ε_{app} of 0.46%, which was the failure strain of the aligned MWCNT/epoxy composite.

Figure(s)

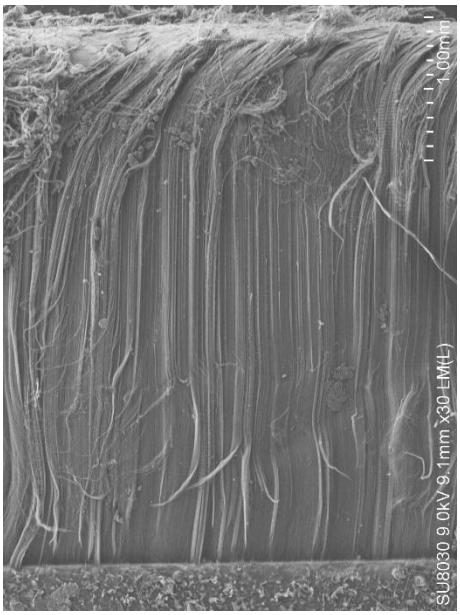

Figure 1

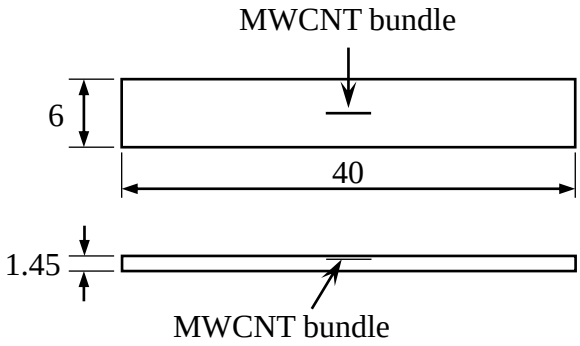

(a) Unit: mm

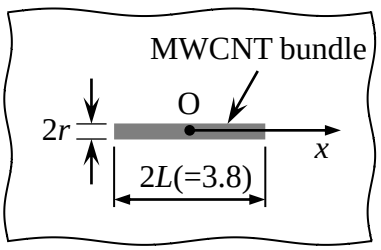

(b)

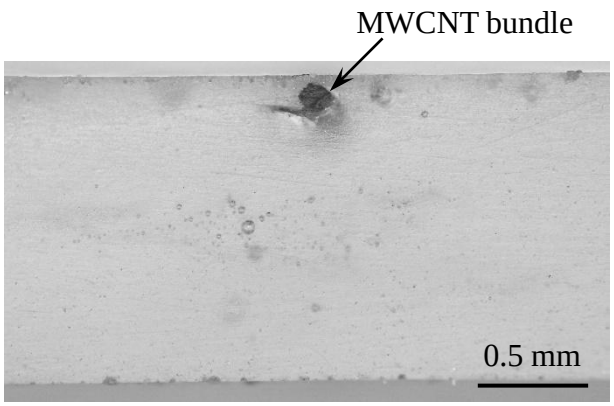

(c)

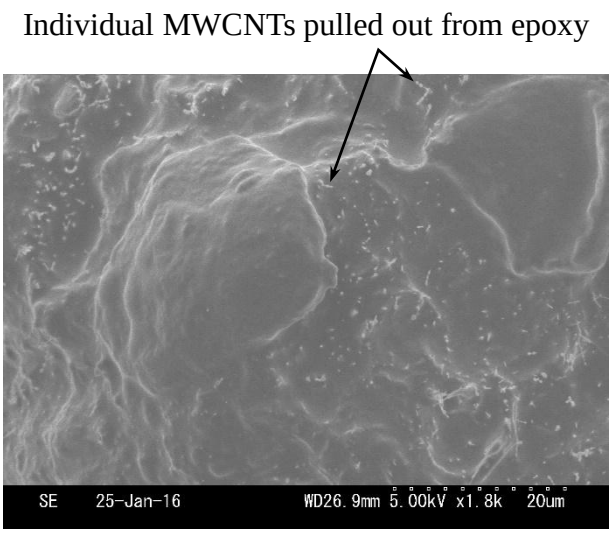

(d)

Figure 2

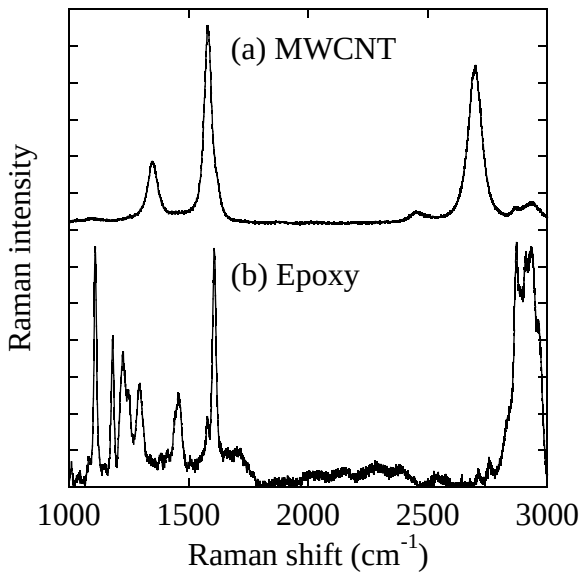
(a) MWCNT
(b) Epoxy
Raman intensity
1000
1500
2000
2500
3000
Raman shift (cm-1)

Figure 3

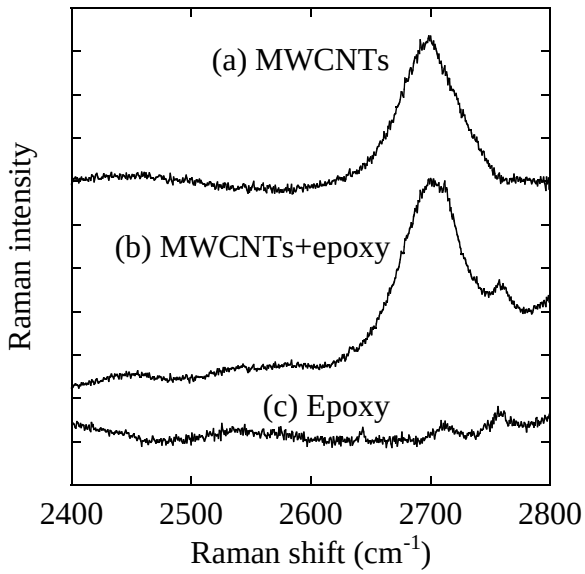
(a) MWCNTs
(b) MWCNTs+epoxy
(c) Epoxy
Raman intensity
2400
2500
2600
2700
2800
Raman shift (cm-1)

Figure 4

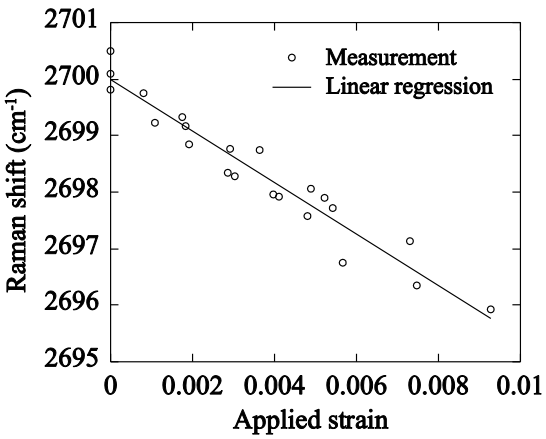
2701
2700
2699
2698
2697
2696
2695
Raman shift (cm-1)
0
0.002
0.004
0.006
0.008
0.01
Applied strain
Measurement
Linear regression

Figure 5

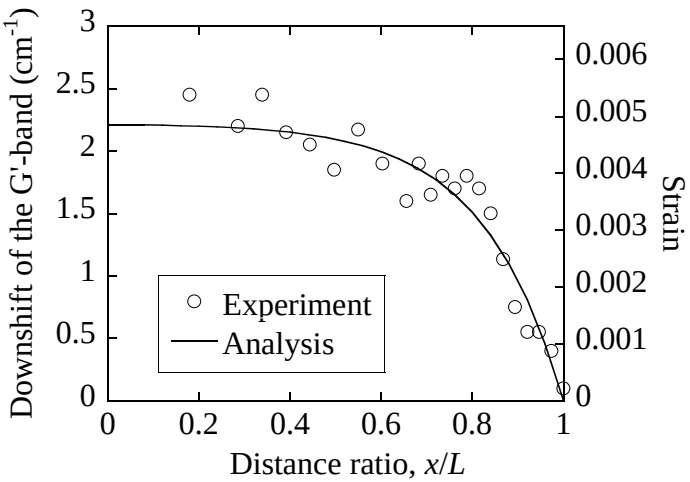
Downshift of the G'-band (cm^{-1})
Strain
Distance ratio, x/L
Experiment
Analysis
0
0.5
1
1.5
2
2.5
3
0.001
0.002
0.003
0.004
0.005
0.006
0.2
0.4
0.6
0.8

Figure 6

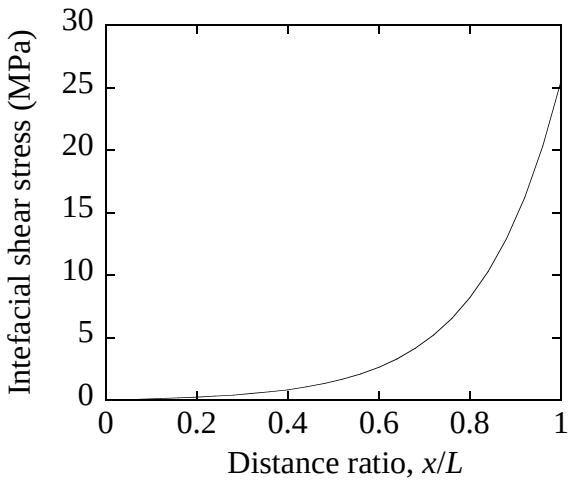
Intefacial shear stress (MPa)
30
25
20
15
10
5
0
0
0.2
0.4
0.6
0.8
1
Distance ratio, x/L

Figure 7

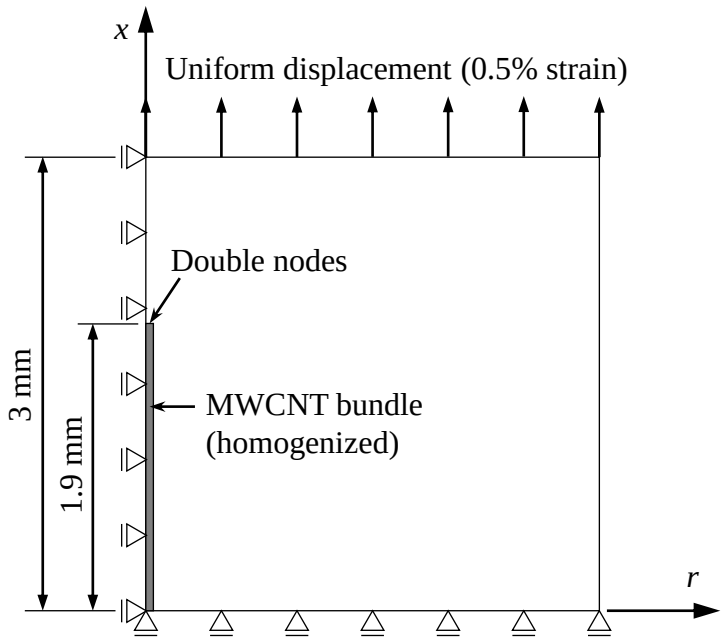

(a) Schematic

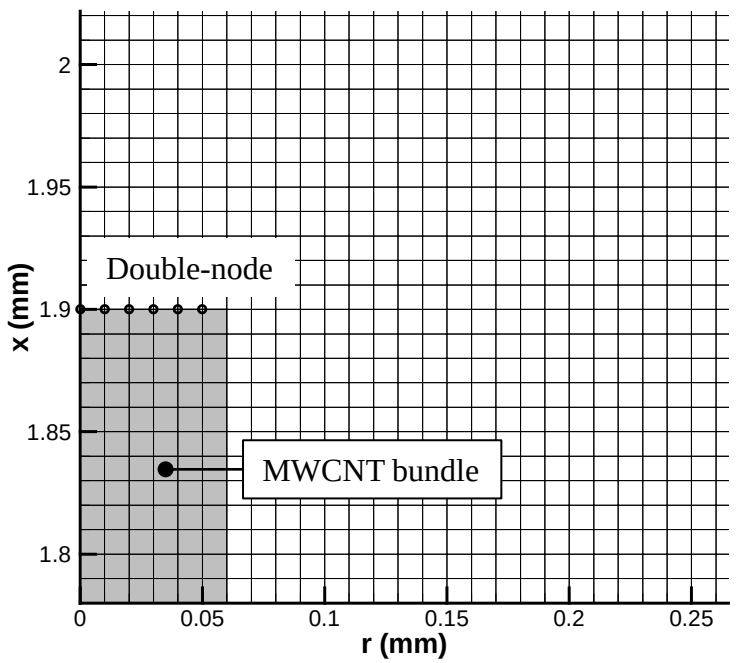

(b) Magnified view of the finite-element model (bundle radius r=60 μm)

Figure 8

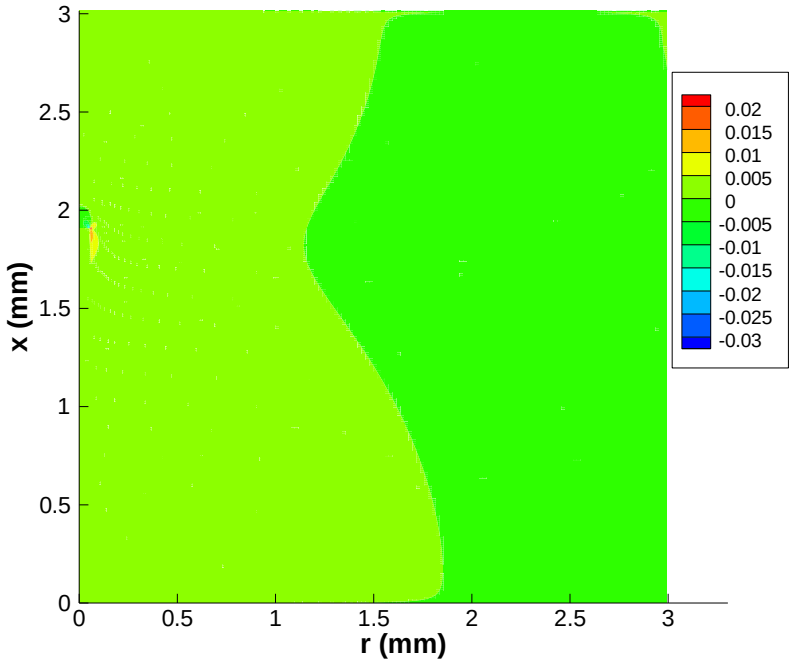

(a) Contour plot

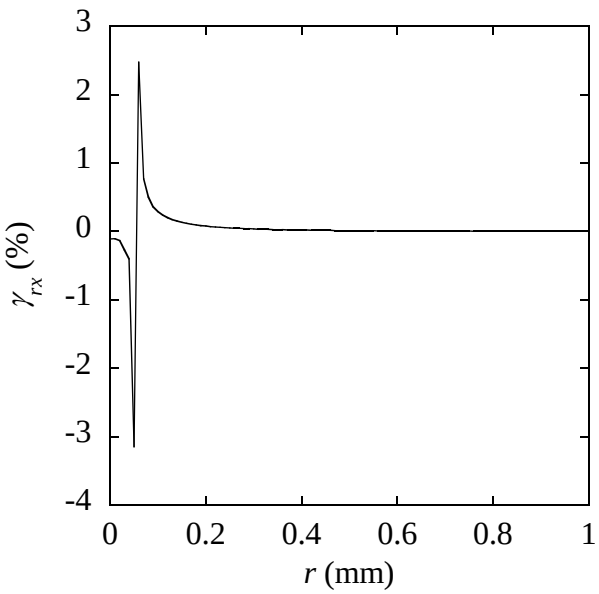

(b) γ_{rx} distribution at the top of the bundle (x = 1.9 mm)

Figure 9

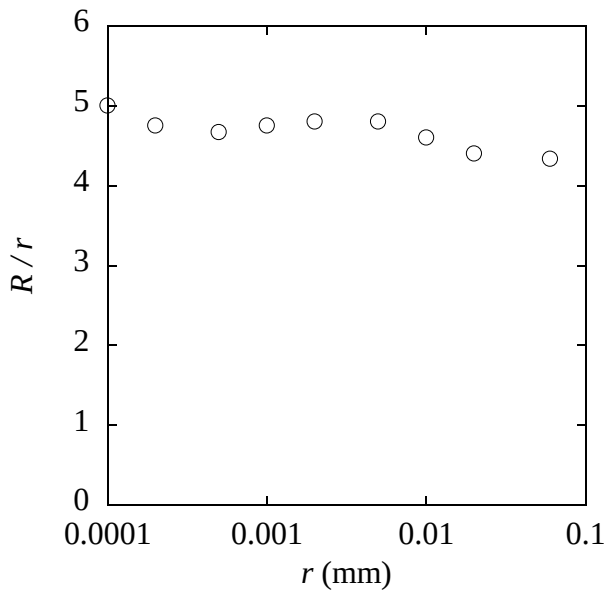

Figure 10